ELSEVIER

Journal of Biomechanics 37 (2004) 1263–1269

JOURNAL OF BIOMECHANICS

www.elsevier.com/locate/jbiomech
www.JBiomech.com

Reassessment of brain elasticity for analysis of biomechanisms of hydrocephalus

Zeike Taylor, Karol Miller*

School of Mechanical and Materials Engineering, The University of Western Australia, 35 Stirling Highway, Crawley/Perth, WA 6009, Australia

Accepted 19 November 2003

Abstract

This paper presents results from a finite element study of the biomechanics of hydrocephalus, with special emphasis on a reassessment of the parenchyma elastic modulus. A two-dimensional finite element model of the human brain/ventricular system is developed and analysed under hydrocephalic loading conditions. It is shown that the Young's modulus of the brain parenchyma used in previous studies (3000–10000 Pa) corresponds to strain rates much higher than those present in hydrocephalic brains. Consideration of the brain's viscoelasticity leads to the derivation of a considerably lower modulus value of approximately 584 Pa.

Keywords: Hydrocephalus; Brain; Mechanical properties; Finite element method

1. Introduction

Hydrocephalus is a disorder of the brain associated with disruption to the flow of cerebrospinal fluid (CSF). CSF is produced by the choroid plexus, within the lateral ventricles of the brain, and under normal conditions is then circulated through the third and fourth ventricles and the spinal cord, and finally absorbed within the sub-arachnoid space (SAS) (Nolte, 1993). In a hydrocephalic brain, an obstruction may block this flow and prevent extrusion of CSF from the lateral ventricles. Consequently, ventricular fluid pressure increases and forces expansion of the ventricle walls. Being confined by the rigid skull (except in infantile cases) the periventricular brain parenchyma is compressed, and in acute cases, destroyed. Additionally, significant oedema is observed in the periventricular material, particularly in the regions of the frontal and occipital horns, as the increased ventricular pressure forces elevated permeation of the CSF through the surrounding tissue. Full development time for the disease is seen to be around 4 days (Nagashima et al., 1987) (Fig. 1).

There has been significant work directed at formulating mathematical descriptions of the biomechanisms involved (e.g. Hakim, 1971; Nagashima et al., 1987; Kaczmarek et al., 1997), and simulating the deformation and diffusion behaviour of affected brains. Of central importance to any such efforts is the incorporation of a realistic constitutive model for the brain material itself. Most work in this area has relied on variations of the biphasic description introduced by Hakim (1971). The material is assumed to consist of an elastic solid skeleton (neurons and neuroglia), permeated by a fluid, interpreted as interstitial fluid and CSF seeping from ventricles to SAS. The fluid phase is allowed to flow within the solid under an imposed pressure gradient, and frictional interaction with the solid results in deformation of this phase.

Whilst Kaczmarek et al. (1997) obtained an analytical solution to a simplified geometric configuration, it is generally necessary to implement numerical approximations for the generation of more realistic hydrocephalus simulations. Specifically, the flexibility of the finite element method has made it the focus of great attention in the area. Nagashima et al. (1987) produced the first example of such an analysis, utilising a linear elastic approximation for the solid phase. Further work was carried out by Tada et al. (1990) and Peña et al. (1999), with both being based heavily on the original principles set out by Nagashima et al. It is worth noting that the

*Corresponding author. Tel.: +61-8-9380-7323; fax: +61-8-9380-1024.
E-mail address: kmiller@mech.uwa.edu.au (K. Miller).
URL: http://www.mech.uwa.edu.au/kmiller.

0021-9290/$ - see front matter © 2004 Elsevier Ltd. All rights reserved.
doi:10.1016/j.jbiomech.2003.11.027

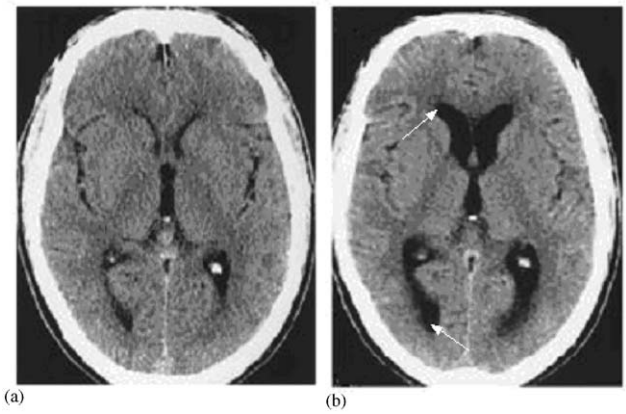

Fig. 1. CT scans of (a) normal ventricular configuration, and (b) dilated ventricles in a hydrocephalic brain. *Source*: Wang et al. (1999). Arrows indicate the frontal (top) and occipital (bottom) horns.

known inability of the biphasic approach to account for strong stress–strain rate-dependence (Miller, 1998) does not affect the applicability of the method in the study of hydrocephalus because the considered strain rates are very close to zero.

This work develops further the investigations mentioned above, and incorporates revised material parameters based on results from the hyper-viscoelastic material model developed by Miller (1999). As a result of the high strain-rate dependence of the brain material, and the extremely slow loading characteristic of the disease, it is shown that brain parenchyma elastic modulus values typically quoted in the literature are not applicable to the study of hydrocephalus.

2. Mathematical model of biphasic continuum

2.1. General principles of the biphasic theory

Following the work of Nagashima et al. (1987) and Peña et al. (1999), the biphasic nature of the brain tissue may be modelled using the principles of Biot's consolidation theory (Biot, 1941), as set out below.

(i) Terzaghi's effective stress principle;
(ii) Darcy's law for fluid flow through a porous medium;
(iii) Conservation of mass of wetting fluid;
(iv) Equilibrium of the medium;
(v) A constitutive relation for the solid phase.

Details of the theory are not elaborated here. Relevant equations for effective stress, Darcy's law, fluid mass conservation, and equilibrium may be found in Bowen (1976). The constitutive modelling of the solid phase is discussed in more detail in Section 2.2.

2.2. Constitutive modelling of biphasic continuum

2.2.1. Solid phase elasticity

Studies have shown brain material properties to be clearly non-linear and strain rate-dependent (Miller, 1999; Miller and Chinzei, 1997). It is important to consider what range of strains and strain rates is important for modelling brain structural diseases, such as hydrocephalus.

The strain rates produced during the development of hydrocephalus are so low that in this study we assume that the strain rate-dependency of the mechanical properties of the brain tissue can be omitted and a limiting hyperelastic response to quasi-static loading (strain rate approaching zero) assumed. Also the non-linear stress–strain relationship is, in our opinion, not critical for the validity of conclusions of this study. Computer simulations discussed later show that the great majority of hydrocephalic brain volume is in the state of compressive strain of just under −3%. For strain of −3% the difference between stress predicted by a non-linear model (Miller, 1999) and a linear model applied in this study is about 1.5% (−29.62 Pa given by non-linear hyperelastic model versus −30.06 Pa given by the linear model). In view of the fact that strain rate-dependence effects are the main focus of the study, and incorporation of non-linear stress–strain characteristics would complicate the results unnecessarily, in this paper we approximate the behaviour of the solid phase with a linear constitutive model with constant Young's modulus, E:

$$\sigma_{\text{eff}} = \mathbf{D}\varepsilon_{\text{eff}}, \tag{1}$$

where $\boldsymbol{\varepsilon}_{\text{eff}}$ is the effective (Almansi) strain, $\boldsymbol{\sigma}_{\text{eff}}$ is the effective (Cauchy) stress, and $\mathbf{D}$ is given by

$$\mathbf{D} = \frac{E}{(1+v)(1-2v)} \times \begin{bmatrix} 1-v & v & v & 0 & 0 & 0 \\ v & 1-v & v & 0 & 0 & 0 \\ v & v & 1-v & 0 & 0 & 0 \\ 0 & 0 & 0 & \frac{1-2v}{2} & 0 & 0 \\ 0 & 0 & 0 & 0 & \frac{1-2v}{2} & 0 \\ 0 & 0 & 0 & 0 & 0 & \frac{1-2v}{2} \end{bmatrix}, \tag{2}$$

where E is the Young's modulus and ν the Poisson's ratio.

This is a valid modelling technique even when finite deformations are considered. In such case one should choose carefully appropriate, energetically conjugate, stress and strain measures (Bathe, 1996). In this study we chose to measure stress and strain with respect to the

deformed (current) configuration, using Cauchy stress and Almansi strain.

For an essentially strain rate-dependent material such as brain parenchyma, selection of the elastic modulus should be representative of the particular strain rate condition present in the system.

2.2.2. Hyper-viscoelastic model of brain tissue

Several efforts have been made to establish an analysis framework allowing for both finite strains in brain material, and the time-dependence of the material (Mendis et al., 1995; Miller and Chinzei, 1997; Miller, 1999). Miller (1999) proposed a hyperelastic, linear viscoelastic single-phase model, suitable for application in finite element procedures, in the form of a polynomial strain energy function with time-dependent coefficients:

$$W = \int_0^t \left\{ \sum_{i+j=1}^{N} \left[C_{ij0} \left(1 - \sum_{k=1}^{n} g_k (1 - \mathrm{e}^{-(t-\tau)/\tau_k}) \right) \right] \times \frac{\mathrm{d}}{\mathrm{d}\tau} [(J_1 - 3)^i (J_2 - 3)^j] \right\} \mathrm{d}\tau, \quad (3)$$

where C_{ij0} are material parameters, J_1 and J_2 are strain invariants, τ_k are characteristic times, g_k are relaxation coefficients and N is taken to be 2 in this case. An important result from the hyperelastic component of Eq. (3) is that the instantaneous shear modulus, μ_0, is related to the first-order polynomial coefficients, C_{100} and C_{010}:

$$\mu_0 = 2(C_{100} + C_{010}). \quad (4)$$

The shear modulus relates to the Young's modulus of the material as follows:

$$\mu_0 = \frac{E_0}{2(1 + \nu_{\mathrm{hyper}})}, \quad (5)$$

where ν_{hyper} is Poisson's ratio for the hyperelastic continuum. Assuming incompressibility of the medium as a whole ($\nu_{\mathrm{hyper}} \approx 0.5$), a relation between instantaneous tissue elasticity (which may be used as an estimate of elastic modulus for the linear model) and the polynomial strain energy coefficients is produced:

$$E_0 = 6(C_{100} + C_{010}). \quad (6)$$

Using the values obtained by Miller (1999), we obtain $E_0 = 3156\,\mathrm{Pa}$. This is around the same order of magnitude as values generally quoted in the literature (Nagashima et al., 1987; Kaczmarek et al., 1997; Peña et al., 1999).

It is based, however, on the assumption of a strain rate of around $0.64\,\mathrm{s}^{-1}$ (Miller and Chinzei, 1997). Therefore, the value of 3156 Pa as an estimate of solid phase elasticity is *not* valid for situations where strain rates are very low.

2.2.3. Revised elastic material parameters

Biphasic materials can exhibit highly transient responses to mechanical loading, i.e. apparent elastic modulus may be both time- and load rate-dependent. Initial loading of the material will be supported by an immediate increase in pore pressure, but if redistribution of fluid within the material skeleton is allowed to occur (over time), the loading must progressively be supported through deformation of the solid phase. Clearly, then, the apparent elastic modulus will not remain constant.

As indicated in Section 2.2.2, a value for the elastic modulus may be obtained from the first-order hyperelastic polynomial coefficients, C_{100} and C_{010}, via Eq. (6). These values represent the *instantaneous* elasticity and hence are realistically only valid for relatively high strain rates, e.g. the ones encountered during neurosurgery ($\sim 10^{\circ}\,\mathrm{s}^{-1}$), (Miller, 1999). The brain material loading under hydrocephalic conditions, however, is extremely slow, typically progressing to full development over a period of days. Consequently, we may consider the limiting case for the relaxation component of Eq. (3):

$$\lim_{t \to \infty} g_k (1 - \mathrm{e}^{-(t-\tau)/\tau_k}) = g_k. \quad (7)$$

Hence, the *relaxed* hyperelastic coefficients are given by

$$C_{ij\infty} = C_{ij0} \left(1 - \sum_{k=1}^{n} g_k \right). \quad (8)$$

Using $n = 2$, Miller (1999) quotes values of $C_{010} = C_{100} = 263\,\mathrm{Pa}$, $g_1 = 0.450$, and $g_2 = 0.365$. Eq. (8) then gives the *relaxed* hyperelastic coefficients $C_{10\infty} = C_{01\infty} = 48.7\,\mathrm{Pa}$. Incorporating these revised parameters, Eq. (6) yields the modified elastic modulus:

$$E_\infty = 6(C_{10\infty} + C_{01\infty}) = 584.4\,\mathrm{Pa}.$$

The above value is now suitable for use in the simulation of hydrocephalus. This represents a significant reduction in stiffness and demonstrates the importance of understanding and accounting for the essential strain rate dependency of brain material properties.

Permeability, $k = 1.59 \times 10^{-7}\,\mathrm{m/s}$, and Poisson's ratio, $\nu_{\mathrm{solid}} = 0.35$, are obtained from Kaczmarek et al. (1997), and the initial void ratio for the material is taken as 0.2 (Nagashima et al., 1987). It is worth noting that the Poisson ratio, ν_{hyper}, defined in Section 2.2.2. above is different to the ratio, ν_{solid}, defined here. This arises from the fact that two different modelling approaches have been employed. In the first instance, the material was treated as a single phase hyperelastic continuum, so that $\nu_{\mathrm{hyper}} = 0.5$ reflects the fact that *as a whole*, the material is essentially incompressible. When in the second case the material is treated as a biphasic continuum, the Poisson ratio of $\nu_{\mathrm{solid}} = 0.35$ reflects the relative compressibility of the material's *solid phase*,

which allows fluid to be absorbed or exuded from the solid matrix. The first ratio, then, refers to the entire fluid saturated material, while the second refers to the material's drained condition.

The fluid phase is considered to be an incompressible, inviscid fluid with mechanical properties as for water.

Recent work by Ozawa et al. (2001) showed no significant difference between white and grey matter elasticity, and so homogeneity and isotropy are assumed for the entire brain. The presented mathematical formulation is more general than those used in the studies by Nagashima et al. (1987) and Kaczmarek et al. (1997) whose formulations are essentially linear. Kaczmarek's finite deformation results were obtained by superposition of the small-strain solutions.

3. Finite element simulation

A two-dimensional finite element model (FEM) of the brain/ventricle system was developed to assess the elastic modulus revision presented. The model used a linear elastic material formulation for the solid phase of the brain, and incorporated the revised elastic parameter, $E_\infty = 584.4\,\text{Pa}$.

3.1. Geometry and meshing

Construction and meshing of the geometry was performed using MSC/PATRAN pre-processor software (MSC/PATRAN, 2000). The model consisted of 344 8-node quadrilateral elements of type CPE8RP (ABAQUS/Standard, 2001), and 1126 nodes. Fig. 2(a) shows the undeformed mesh used in the model.

Model geometry was obtained from a horizontal cross-section presented in the anatomic atlas of Talairach and Tournoux (1988). The section was taken at 20 mm above a reference defined by the anterior and posterior commissures (refer to Talairach and Tournoux, 1988). Macroscopic undulations of the brain surface were ignored for simplicity, and only a gross outline of the ventricular and surface boundaries were used. Considering the symmetry about the midline, only the right hemisphere was analysed.

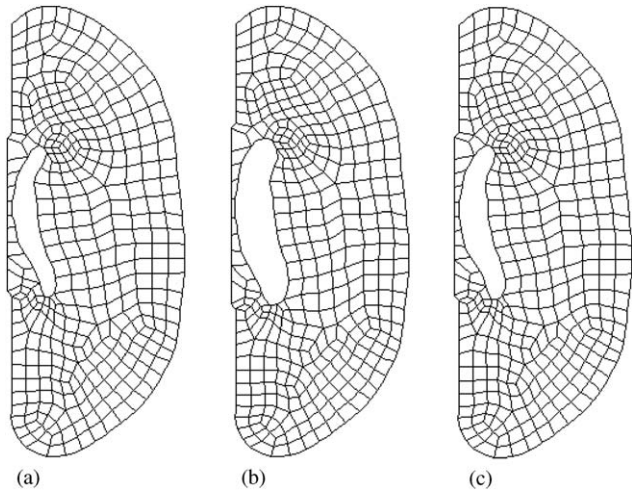

Fig. 2. Comparison of (a) undeformed mesh with (b) deformed mesh using $E_\infty = 584.4\,\text{Pa}$, and (c) deformed mesh using $E = 10\,\text{kPa}$.

3.2. Boundary conditions

Pore pressure was fixed at zero at the skull boundary to ensure outward radial CSF flow and drainage in the SAS. As mentioned, CSF is produced in the lateral ventricles, and absorbed almost entirely in the SAS (Nolte, 1993). A pressure gradient then exists between these two regions such that resulting fluid flow is from ventricles to SAS, i.e. maximum pressure is found in the ventricles, and minimum pressure in the SAS. In the case of a hydrocephalic brain, some obstruction inhibits this fluid flow, leading to an increase in the pressure gradient. A reasonable estimate for this elevated gradient is approx. 3000 Pa (Peña et al., 1999). This is then implemented by setting ventricular fluid pressure to 3 kPa and SAS fluid pressure to 0 kPa.

The outer brain surface was assumed fixed to the skull and so surface nodes are constrained in all directions. Along the midline boundary, nodes are constrained in the horizontal direction (due to the presence of the left hemisphere), but are allowed to displace vertically.

3.3. Loading

Loading of the ventricular wall was in the form of a distributed fluid pressure over the surface. As indicated above, the pressure magnitude was set to 3 kPa, in line with other work by Peña et al. (1999) and Nagashima et al. (1987).

3.4. Analysis

Model solutions were obtained using ABAQUS/Standard finite element software (ABAQUS/Standard, 2001). Consolidation analyses may be performed using ABAQUS' SOILS procedure. This procedure is capable of solving fully non-linear, finite deformation, poroelastic problems, and has been shown to perform well in hydrated soft tissue simulations (Wu et al., 1998). As mentioned, the total development time for hydrocephalus was taken as 4 days (345600 s).

3.5. Mesh convergence study

An *h*-refinement technique was used to assess the mesh convergence of the model. The model was re-meshed using (i) 641 elements and 2057 nodes, and (ii) 2324 elements and 7232 nodes and reanalysed under the

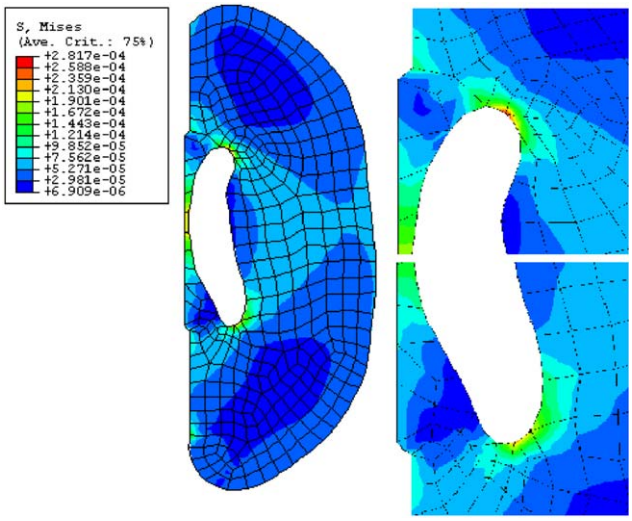

Fig. 3. Von Mises stress distribution (MPa) in the model using $E_\infty = 584.4\,\text{Pa}$.

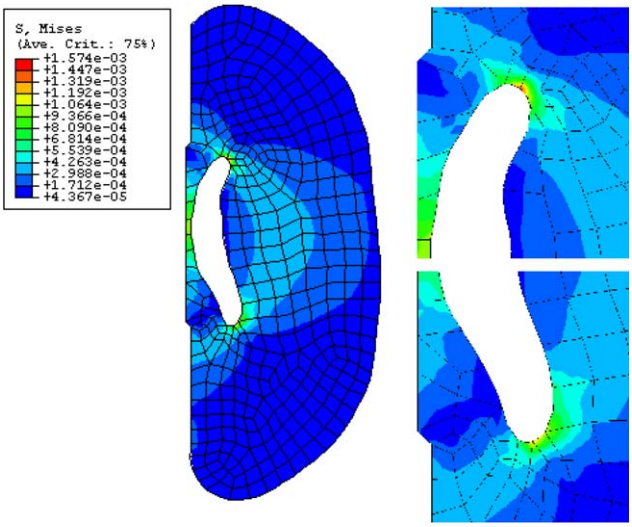

Fig. 4. Von Mises stress distribution (MPa) in the model using $E = 10\,\text{kPa}$.

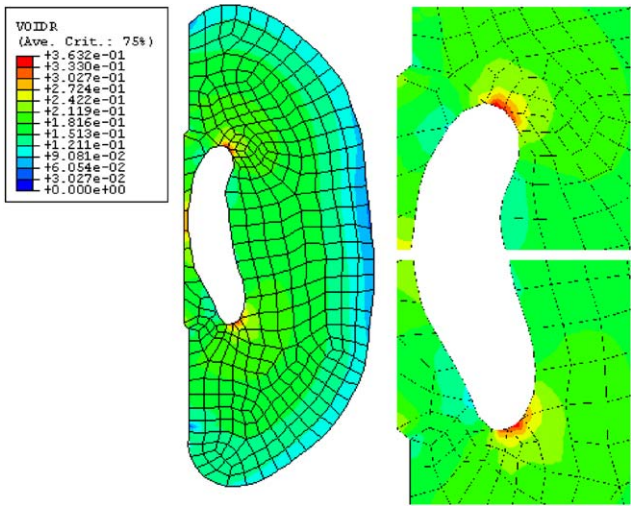

Fig. 5. Void ratio distribution in the deformed model with $E_\infty = 584.4\,\text{Pa}$.

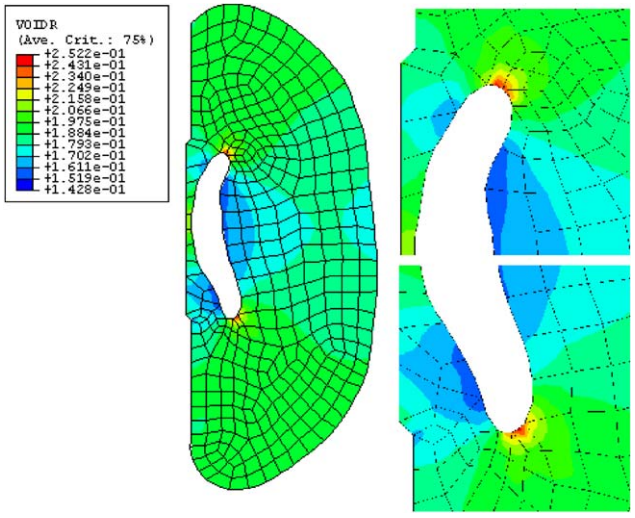

Fig. 6. Void ratio distribution in the deformed model with $E = 10\,\text{kPa}$.

same conditions. Deformation results for the three meshes (original, plus two refined) differed by less than 1%, thus confirming the convergence of the solution.

4. Results

Fig. 2(b) shows the deformed mesh compared with the original configuration. A second simulation was performed using an elastic modulus of 10 kPa in order to compare with the work of Peña et al. The resulting deformation is shown in Fig. 2(c). The pressure across the surface of the ventricle produces an overall expansion of the ventricular space. In particular, there is a pronounced lateral displacement of the right wall of the ventricle, and a dilation of the ventricle tips (frontal and occipital horns). Using the revised modulus, maximal displacement midway along the ventricle right wall is obtained as 4.79 mm. Using $E = 10\,\text{kPa}$ produces an equivalent displacement of 1.57 mm.

Figs. 3 and 4 show the Von Mises stress distributions for the revised modulus model, and for the 10 kPa model respectively. Relatively high tensile stresses are focused around the frontal and occipital horns with peak stress in these regions around 282 Pa for the former, and 1574 Pa for the latter.

Figs. 5 and 6 show the void ratio distributions in the model after loading—the unloaded void ratio throughout the medium is 0.2. Significant increases around the ventricular horns are apparent in both cases. Void ratios in these regions rise to as much as 0.363 using the revised

modulus—a rise of 0.163 (81.5%), and 0.252 using $E = 10\,\text{kPa}$—a rise of 0.052 (26%).

5. Discussion and conclusions

It is interesting to note that the deformation produced using $E = 10\,\text{kPa}$ appears to be somewhat less than that observed in clinical cases (e.g. Fig. 1). Two explanations seem plausible: the hydrocephalic ventricular pressure was underestimated, or the Young's modulus was overestimated. The significantly larger deformation observed with the revised modulus would seem to imply the latter. It should be noted however, that it is generally difficult to make *quantitative* comparisons between simulated deformations and clinical cases. There are three reasons for this:

1. Degrees of deformation vary considerably from case to case.
2. The true magnitude of the ventricular loading is not well known.
3. There is significant variation in the values of material parameters quoted in the literature, which are further complicated by load rate-dependency.

In spite of this, many qualitative characteristics produced by the model may still be linked to clinical observations.

The dilations of the frontal and occipital horns referred to above are frequently observed in clinical cases (see Fig. 1), and additionally, are usually accompanied by CSF oedema, as evidenced by periventricular lucency (PVL) in the region.

The similarity in the deformation pattern produced with both moduli points to observations by Peña et al. (1999) and Nagashima et al. (1987) that fields of this type are strongly dependent on the geometric arrangement of the ventricles. This is particularly demonstrated here where two geometrically identical models with elasticity differing over an order of magnitude exhibit essentially the same deformation pattern.

Of significant interest in the stress distribution results are the relatively high tensile stresses focused around the ventricular horns. These are a result of the dilation referred to above. As observed by Peña et al. (1999), the concavity of these regions means ventricular fluid pressure acts to *stretch* the local material. A consequence of this stretching is that the ependymal cells, which line the ventricle, are disrupted. Under normal conditions, these closely packed cells exhibit a substantially lower permeability than the surrounding material (Peña et al., 1999). This prevents extensive diffusion of CSF into the brain material. When this material is stretched however, its pores will distend and permeability should increase, thus promoting fluid oedema in these regions. This is in line with observations of PVL in MRI scans of hydrocephalic brains.

A further result that points to the development of PVL is the distribution of void ratio in the material. A comparison of Figs. 3,5 and 4,6 shows that the tensile stress concentrations in the horns are reflected as increases in the void ratio of these regions. This tends to confirm the statement above that tensile stress is accompanied by distension of the extra-cellular space. As the medium remains fully saturated, any increase in void ratio corresponds to an increase in the fluid content in that region. Literally, the areas with increased void ratio around the ventricle horns may be identified as areas of fluid oedema.

It is observed, then, that the *distribution* of solution fields such as displacement, stress, and void ratio produced by this model may be seen to reflect some of the clinical attributes of the disease. Comparison of the results produced using the revised elastic modulus with those of an existing value used in similar simulations shows that significant variations in field magnitudes are generated when consideration of the material's viscoelastic properties is made. The degree of magnitude variation involved highlights the importance of using a modulus value appropriate to the specific analysis. Furthermore, in light of the relatively larger deformations produced with the revised modulus—in line with large clinically observed ventricular expansions, $E_\infty = 584.4\,\text{Pa}$ is presented as a more appropriate value for low strain rate simulations of this kind.

Acknowledgements

Financial support of the Australian Research Council and the UWA Grants scheme is gratefully acknowledged.

References

ABAQUS/Standard, 2001. Version 6.2, Hibbit, Karlsson & Sorenson, Inc.

Bathe, K.-J., 1996. Finite Element Procedures in Engineering Analysis. Prentice-Hall, Inc, Englewood Cliffs, NJ.

Biot, M.A., 1941. General theory of three dimensional consolidation. Journal of Applied Physics 12, 1244–1258.

Bowen, R.M., 1976. Theory of mixtures. In: Eringen, A.C. (Ed.), Continuum Physics, Vol. III. Academic Press, New York, pp. 1–127.

Hakim, S., 1971. Biomechanics of hydrocephalus. Acta Neurologica Latinoamericana 17, 169–174.

Kaczmarek, M., Subramaniam, R.P., Neff, S.R., 1997. The Hydromechanics of hydrocephalus: steady-state solutions for cylindrical geometry. Bulletin of Mathematical Biology 59 (2), 295–323.

Mendis, K.K., Stalnaker, R.L., Advani, S.H., 1995. A Constitutive relationship for large deformation finite element modelling of brain tissue. Journal of Biomechanical Engineering—Transactions of the ASME 117, 279–285.

Miller, K., 1998. Modelling soft tissue using biphasic theory—a word of caution. Computer Methods in Biomechanics and Biomedical Engineering 1, 261–263.

Miller, K., 1999. Constitutive model of brain tissue suitable for finite element analysis of surgical procedures. Journal of Biomechanics 32, 531–537.

Miller, K., Chinzei, K., 1997. Constitutive modelling of brain tissue: experiment and theory. Journal of Biomechanics 30 (11/12), 1115–1121.

MSC/PATRAN, 2000. Version 9.0, MSC Software Inc.

Nagashima, T., Tamaki, N., Matsumoto, S., Horwitz, B., Seguchi, Y., 1987. Biomechanics of hydrocephalus: a new theoretical model. Neurosurgery 21 (6), 898–904.

Nolte, J., 1993. The human brain: an introduction to its functional anatomy. Mosby-Year Book, Inc, Missouri.

Ozawa, H., Matsumoto, T., Ohashi, T., Sato, M., Kokubun, S., 2001. Comparison of spinal cord gray matter and white matter softness: measurement by pipette aspiration method. Journal of Neurosurgery 95 (Suppl. 2), 221–224.

Peña, A., Bolton, M.D., Whitehouse, H., Pickard, J.D., 1999. Effects of brain ventricular shape on periventricular biomechanics: a finite-element analysis. Neurosurgery 45 (1), 107–118.

Tada, Y., Matsumoto, R., Nishimura, Y., 1990. Mechanical modellings of the brain and simulation of the biomechanism of hydrocephalus. JSME International Journal 33 (2), 269–275.

Talairach, J., Tournoux, P., 1988. Co-planar stereotaxic atlas of the human brain. Thieme Medical Publishers, Inc, New York.

Wang, M.C., Escott, E.J., Breeze, R.E., 1999. Posterior fossa swelling and hydrocephalus resulting from hypertensive encephalopathy: case report and review of the literature. Neurosurgery 44 (6), 1325–1327.

Wu, J.Z., Herzog, W., Epstein, M., 1998. Evaluation of the finite element software ABAQUS for biomechanical modelling of biphasic tissues. Journal of Biomechanics 31, 165–169.